Inducement Mechanism and Control of Self-acidification in Elemental Sulfur Fluidizing Bioreactor

Author names and affiliations:

Yi-Lu Sun [1, a], Jia-Yu Wang [1, b], Huu Hao Ngo [c], Wei Wei [c], Wenshan Guo [c], Xue-Ning Zhang [*, a], Hao-Yi Cheng [d], Ji-Xian Yang [b], Ai-Jie Wang [a, d]

[a] Key Laboratory of Environmental Biotechnology, Research Center for Eco-Environmental Sciences, Chinese Academy of Sciences, Beijing, 100085, China.

[b] School of Environment, Harbin Institute of Technology, Harbin, 150090, China.

[c] Centre for Technology in Water and Wastewater, School of Civil and Environmental Engineering, University of Technology Sydney, Sydney, New South Wales 2007, Australia.

[d] State Key Laboratory of Urban Water Resources and Environment, Harbin Institute of Technology Shenzhen, Shenzhen, 518055, China.

[1]The authors contributed equally to this study.

***Corresponding author.**

Xue-Ning Zhang: xnzhang@rcees.ac.cn

Inducement Mechanism and Control of Self-acidification in Elemental Sulfur Fluidizing Bioreactor

Abstract

The sulfur fluidizing bioreactor (S^0FB) has significant superiorities in treating nitrate-rich wastewater. However, substantial self-acidification has been observed in engineering applications, resulting in frequent start-up failures. In this study, self-

acidification was reproduced in a lab-scale S^0FB. It was demonstrated that self-acidification was mainly induced by sulfur disproportionation process, accounting for 93.4% of proton generation. Supplying sufficient alkalinity to both the influent (3000 mg/L) and the bulk (2000 mg/L) of S^0FB was essential for achieving a successful start-up. Furthermore, the S^0FB reached 10.3 kg-N/m^3/d of nitrogen removal rate and 0.13 kg-PO_4^{3-}/m^3/d of phosphate removal rate, respectively, surpassing those of the documented sulfur packing bioreactors by 7–129 times and 26–65 times. This study offers a feasible and practical method to avoid self-acidification during restart of S^0FB and highlights the considerable potential of S^0FB in the treatment of nitrate-rich wastewater.

Keywords: autotrophic denitrification, disproportionation, alkalinity, phosphate, nitrate-rich wastewater

1. Introduction

Nitrogen is recognized to contribute to surface water eutrophication, posing a significant threat to aquatic systems (Dong et al., 2023). Stringent emission standards and the pursuit of sustainable practices have greatly propelled the advancement of nitrogen removal technologies. Biological treatment processes have currently become the most widely utilized and cost-effective solutions for nitrogen removal (Ricardo et al., 2012). However, certain industrial wastewaters from ammunition, pharmaceutical, metal finishing, and nuclear industries (Glass & Silverstein, 1998; Nancharaiah & Venugopalan, 2011), contain hundreds to thousands of milligrams per liter of nitrate-nitrogen with a low carbon to nitrogen (C/N) ratio (Kim et al., 2004b). This presents a challenge to the efficiency of biological treatment. Address this issue necessitates the addition of a substantial amount of organic carbon to uphold an effective heterotrophic denitrification process (Gong et al., 2013; Karanasios et al., 2016). However, this results in undesirable operational expenses and carbon dioxide emissions (Sun et al., 2017; Xu et al., 2018).

The sulfur-driven autotrophic denitrification (S^0AD) process, especially through the use of sulfur packing bioreactor (S^0PB), is increasingly being employed in practical engineering to attain reduced operational expenses and accomplish carbon-neutralization objectives (Chen et al., 2022; Wang et al., 2022). However, the efficiency of sulfur utilization severely restricts the performance of S^0PB, primarily due to the low water solubility of sulfur (0.16 μmol/L at 25 °C) (Capua et al., 2017). Furthermore, clogging is inevitable during S^0PB operation and can worsen with increased denitrification efficiency due to the accumulation of decomposed biomass and produced N_2 in the sulfur-packing media (Di Capua et al., 2015). These characteristics determine the unsuitability of using S^0PB for the treatment of nitrate-rich wastewater.

The sulfur fluidizing bioreactor (S^0FB) utilizing micron-sized sulfur particles has proven effective in treating nitrate-rich wastewater, achieving a denitrification rate 2–5 times higher than that of S^0PB (Kim et al., 2004a). This improvement is attributed to the increased active biomass, specific surface area of sulfur particle, and substrate transfer rate (Ozkaya et al., 2019). Despite using thiosulfate instead of elemental sulfur as the electron donor under varying pH, temperature, and nitrate loading conditions has been successfully demonstrated (Di Capua et al., 2017; Zou et al., 2016), its high cost is generally deemed unacceptable, thus limiting its practical application. Instead, adapting sulfur as an economic alternative promotes its potential applications. However, the limited understanding (only 5 studies to date) of the S^0FB results in numerous uncertainties in the subsequent scaling-up process. Moreover, in previous engineering practice, a significant acidification phenomenon was observed during the restart of S^0FB, which significantly caused restart failures and impeded the maintenance of an effective operation of S^0FB in the long run. Therefore, it is essential to bring this

engineering issue back to the laboratory for comprehensively investigating the underlying mechanism and providing feasible solutions.

In this study, a lab-scale S^0FB was used to reemerge the acidification phenomenon in engineering practice. To tackle the problem of acidification, various approaches for providing alkalinity were tested to determine their effectiveness in accomplishing a successful and effective restart of the S^0FB. The fundamental mechanism of acidification occurrence and its impact on the denitrification process were explored through stoichiometric, thermodynamic, and biological analyses. Additionally, the maximum capabilities of the S^0FB for nitrogen and phosphorus removal were investigated. This study aims to improve the comprehension of acidification occurrence and provide feasible solutions to promote S^0FB applications.

2. Materials and Methods

2.1 Sulfur fluidizing bioreactor

A lab-scale S^0FB with a diameter of 40 mm and a working volume of 1.5 L was assembled (see Supplementary Materials). Sulfur particles, averaging 450 μm in diameter and obtained from a pilot-scale S^0FB that remained idle after 2 months robust operation, were filled into the S^0FB to a depth of 255 mm. The expansion rate of sulfur particles during fluidization was maintained at 150% with a recirculation rate of 266.7 ml/min using a self-priming pump (LS-0412, China). The S^0FB was operated in a continuous inflow mode, with synthetic wastewater (see Supplementary Materials) introduced into the influent port at the base of the S^0FB. The temperature was maintained at 30±1 ℃ through the use of heating wires surrounding the reactor and heaters in the influent tank.

2.2 Start-up and operation of the sulfur fluidizing bioreactor

The S^0FB experienced three rounds of start-up followed by a long-term stable operation, as described in Table 1. During each round of start-up, the S^0FB was initially filled with tap water containing approximately 2.5±0.5 mg-N/L of nitrate and 150±10 mg/L of alkalinity. Subsequently, tap water amended with nitrate, bicarbonate, and phosphate was continuously fed into the S^0FB with an empty bed contact time (EBCT) of 40 min. During the 1st and 2nd rounds of start-up, alkalinity of 285.8±48.0 mg/L and 2235.3±106.8 mg/L was solely supplied to the influent, while in the 3rd round start-up, 3303.3±178.4 mg/L and 2000±50 mg/L of alkalinity were supplied to both the influent and the S^0FB bulk, respectively. Following a successful start-up (the 3rd round), the S^0FB was continuously operated with gradual increases in the influent nitrate from 49.9±1.4 to 314.5±16.1 mg-N/L and phosphate from 1.0±0.04 to 4.2±0.1 mg/L. Influent and effluent water samples were daily collected for chemical analysis.

2.3 Chemical analysis

Water samples were collected using a 0.22 μm membrane filter. Anions (nitrite, nitrate, phosphate, and sulfate) were measured using an ion chromatograph (883 Basic IC plus, Metrohm, Swizerland) equipped with a Metrosep A Supp 5−250 column (Metrohm, Swizerland). pH values were measured using a pH meter (pH-Electrode SenTix 940–3, WTW GmbH, Germany). Dissolved oxygen (DO) and temperature values were measured using a multi-parameter portable meter (WTW Multi 3620 IDS).

2.4 Microbial community analysis

SEM images were obtained using a SU-8020 scanning microscope (Hitachi, Japan) to visually inspect the microorganisms on the sulfur particle surface (see Supplementary Materials). Biomass samples were collected from the sulfur particles prior to start-up (SU) and post stable operation (SO) for the purpose of conducting microbial community analysis. The details of biomass pre-treatment, primers, and high-throughput sequencing can be found in the previous study (Zhang et al., 2022b). The raw sequences of all samples have been deposited in GenBank database (NCBI, www.ncbi.nlm.nih.gov/) with an accession number PRJNA1030742.

3. Results and Discussion

3.1 Self-acidification in the sulfur fluidizing bioreactor

The S^0FB experienced three start-up rounds with different alkalinity feed conditions, as described in Table 1. During the 1st round of start-up, the effluent demonstrated a gradual increase in nitrate concentration from 1.1 to 4.6 mg-N/L over the first 4 days (Fig. 1A). Simultaneously, there was a considerable decrease in pH from 6.8 to 3.0 (Fig. 1C), strongly inhibiting the activities of denitrification reductases (Liu & Koenig, 2002; Oh et al., 2000). Subsequently, the effluent nitrate continued to increase, reaching 28.9 mg-N/L on day 19, with higher influent levels of nitrate (46.6±2.2 mg-N/L) and alkalinity (2044.6±107.4 mg/L). Consequently, this resulted in an ineffective nitrate removal efficiency of only 33%, indicating the failure of the start-up. To mitigate substantial acidification, an initial alkalinity of 2235.3±106.8 mg/L was introduced to the influent during the 2nd round of start-up. Effective nitrate removal from 49.4 to 54.5 mg-N/L was achieved within the initial 7 days, accompanied by a moderate decline in pH from 7.0 to 6.7. However, there was a dramatic drop in pH from 6.3 to 4.8 starting from day 8, leading to a continuous increase in nitrate from 2.0 to 26.0 mg-N/L and an accumulation of nitrite up to 6.3 mg-N/L (Fig. 1C) in the effluent, indicating the start-up failed once again. To stabilize the pH, 2000±50 mg/L and 3303.3±178.4 mg/L of alkalinity were introduced into the bulk and influent, respectively, during the 3rd round of start-up. Consequently, effective and stable S^0AD performance was achieved,

maintaining the pH at approximately 8.3±0.1, exhibiting the complete removal of 49.5±1.8 mg-N/L nitrate and minimal accumulation of nitrite. This illustrates the successful start-up of the S^0FB.

During the stable operation period of the S^0FB, the influent nitrate concentration was stepwise increased from 49.9±1.4 mg-N/L to 314.5±16.1 mg-N/L. Generally, nearly complete removal of nitrate was achieved until the influent nitrate concentration reached 314.5±16.1 mg-N/L. Meanwhile, a considerable accumulation of nitrite occurred during the initial days of elevating the influent nitrate concentration, which also exerts bio-toxicity on microorganisms (Di Capua et al., 2019; Ricardo et al., 2006). Under an influent nitrate concentration of 314.5±16.1 mg-N/L, the effluent nitrate gradually increased from 3.9 to 75.4 mg-N/L, with a maximum nitrite accumulation of 219.9 mg-N/L, illustrating that the S^0FB reached its maximum S^0AD process capability at an EBCT of 40 min. Additionally, although a stable pH value was sustained in the S^0FB, variations in pH drop occurred based on the amount of proton production through the S^0AD process (Bai et al., 2023).

3.2 Inducing mechanism of self-acidification

To comprehend the control of self-acidification by various alkalinity addition approaches, the levels of alkalinity consumption were investigated, as shown in Fig. 2. Throughout the 1st round start-up, complete alkalinity consumption was consistently observed, despite the increasing influent alkalinity from 285.8±48.0 to 2044.6±107.4 mg/L (Fig. 2A), corresponding to the notable decline in pH (Fig. 1C). Although initially introducing 2235.3±106.8 mg/L of alkalinity into the influent slowed down the pH drop during the 2nd round start-up, an average effluent alkalinity of 98.8 ± 18.0 mg/L was observed during the initial 7 days. Subsequently, it further decreased to 14.4±7.9 mg/L due to the significant consumption of alkalinity amounting to 2222.0±118.4 mg/L. In contrast, supplying 3303.3±178.4 mg/L of alkalinity to the influent and 2000±50 mg/L directly to the bulk effectively maintained the normal pH and reasonable alkalinity consumption. Over the initial 15 days with 49.5±1.8 mg-N/L of nitrate removal, an average consumption of alkalinity totaling around 861.6±143.2 mg/L was observed, presenting a ratio of alkalinity consumption nitrate removal at 17.3±3.5. Subsequently, the increase in alkalinity consumption coincided with an improvement in nitrogen removal efficiency.

Sulfur autotrophic denitrification is an acidogenic process (Eq. 1) (Bai et al., 2023), which consumes 4.57 mg/L of alkalinity (accounted as $CaCO_3$) for the complete reduction of 1.0 mg-N/L nitrate to dinitrogen gas (Capua et al., 2017). However, the actual alkalinity consumption during the 1st start-up was 1673.8±743.9 mg/L, significantly exceeding the theoretical value of 112.8±31.3 mg/L calculated using the alkalinity consumption ratio of 4.57. This additional alkalinity consumption was

significantly eliminated following the successful start-up of S^0FB, particularly during the stable operation period with a higher nitrate loading. The results indicate that apart from the S^0AD process, other biological processes also substantially contributed to the reduction in alkalinity. Sulfur oxidation by oxygen (S^0OX, Eq. 2) and sulfur disproportionation (S^0DP, Eq. 3) are also identified as acidogenic processes (Finster et al., 1998; Zhang et al., 2021a). To verify whether the oxygen was involved through recirculation to induce the occurrence of the S^0OX process, an experiment of recirculating anaerobic pure water was conducted. As a result, oxygen was indeed induced through the recirculation process but with a rate of only 4.0 mg-DO/d. Considering the DO concentration of approximately 7.4±0.2 mg/L present in the influent as well, the overall alkalinity consumption related to the S^0OX process was calculated to be a maximum of 42.5±1.1 mg/L. This indicates that the S^0OX process did not primarily contributor to the extra alkalinity consumption. Therefore, the remaining possible cause of the remarkable alkalinity consumption was proposed to be the S^0DP process.

Previous reports indicate that S^0DP bacteria are strictly anaerobic microbes incapable of conducting the S^0DP process in the presence of nitrate and nitrite (Lovley & Phillips, 1994). At the beginning of the 1st start-up, due to the dilution by the large recirculation ratio, the concentrations of sulfur-heterologous electron acceptors (SHEAs) in the bulk were quite low, thereby providing an optimal inducing for the S^0DP process (Sun et al., 2023). Moreover, this was reasonable due to the serious acid inhibition in the S^0AD process (Liu & Koenig, 2002; Oh et al., 2000), but not in the S^0DP process, which could remain highly active under pH < 4.5 (Hardisty et al., 2013), similar to the condition in this study. The increased addition of external alkalinity was essential to achieve a robust S^0AD process by maintaining a suitable pH.

$$55S^0 + 50NO_3^- + 38H_2O + 20CO_2 + 4NH_4^+ \rightarrow 4C_5H_7O_2N + 55SO_4^{2-} + 25N_2 + 64H^+ \quad (1)$$

$$S^0 + 1.22O_2 + 0.267CO_2 + 0.018HCO_3^- + 0.057NH_4^+ + 1.10H_2O \rightarrow 0.057C_5H_7O_2N + SO_4^{2-} + 2.04H^+ \quad (2)$$

$$4S^0 + 4H_2O \xrightarrow{\text{unknown enzyme}} SO_4^{2-} + 3HS^- + 5H^+ \quad (3)$$

3.3 Contributions of different pathways to self-acidification.

The total sulfate production from the combined S^0AD, S^0OX, and S^0DP processes was determined, as shown in Fig. 3A. Generally, the influent sulfate concentration ranged from 29.9 to 41.8 mg/L throughout the operation of S^0FB. The effluent sulfate concentration sharply increased to 2404.7 mg/L and 2205.4 mg/L by the end of the 1st and 2nd start-up periods, respectively. In contrast, stable sulfate production was

observed during the successful 3rd start-up, ranging from 1221.6 mg/L to 1272.8 mg/L. Subsequently, it dropped to a lower level of 329.5 mg/L on day 23 and consistently correlated with the nitrogen removal performance.

The observed sulfate production was significantly higher than what would be anticipated from considering only the S^0AD process during each round of start-up. This finding, in agreement with the alkalinity consumption (Fig. 2), further supports the notion that self-acidification primarily stemmed from a reaction other than S^0AD. In addition to alkalinity consumption, the production of sulfate is another shared feature among the S^0AD, S^0OX, and S^0DP processes (Bai et al., 2023; Finster et al., 1998; Zhang et al., 2021a). Based on Eq. 1–3 and the specific reaction conditions, the total sulfate production of 1568.6±731.9 mg/L was contributed by 186.0±51.6 mg/L from S^0AD, 40±1.0 mg/L from S^0OX, and 1342.6±679.3 mg/L from S^0DP, respectively (Fig. 3B). A decrease in sulfate production was noticed as the addition of alkalinity increased, reaching levels comparable to those from the sole S^0AD process during the stable operation period.

The results showed that the S^0AD, S^0OX, and S^0DP processes made varying contributions to self-acidification. By examining the mass balance of alkalinity and sulfate, the contributions of the S^0AD, S^0OX, and S^0DP processes to self-acidification under different operational conditions were calculated, as shown in Fig. 3C. The S^0DP process emerged as the primary driver of self-acidification, accounting for 70.3–93.4% of proton production. This underscores the active metabolism of the S^0DP bacteria, even under acidic conditions, consistent with previous observations (Hardisty et al., 2013). The decrease in S^0DP contribution to 63.7% during the 3rd start-up signaled a decline in S^0DP activity, attributed to sulfur competition with the survival of S^0AD bacteria under suitable pH conditions (Di Capua et al., 2017). During the stable operational period, the S^0DP contribution was significantly reduced to a negligible level, ranging from 17.0% to 11.0%, owing to the presence of SHEAs that significantly inhibited the S^0DP process (Sun et al., 2023b). While the S^0OX process could play a role in self-acidification, its relatively minor contribution, ranging from 1.2 to 5.7%, suggests that it was not a significant inducing factor of self-acidification.

3.4 Maximum capabilities of nitrogen and phosphate removal

Following the successful start-up of S^0FB, the nitrate loading was gradually increased from 1.9±0.08 to 15.1±0.8 kg-N/m^3/d, as depicted in Fig. 4A. Complete total nitrogen (TN) removal was achieved with a TN removal rate of 10.3 kg-N/m^3/d at a nitrate loading of 11.2 kg-N/m^3/d. However, with each subsequent increase in nitrate loading, there was a significant drop in the TN removal rate, attributed to decreased nitrate removal efficiency or increased nitrite accumulation (Fig. 1A and B). Fortunately, the TN removal rate could gradually recover from 1.9 to 4.3 kg-N/m^3/d

between day 24–30, and rapidly increased from 0.8 to 9.2 kg-N/m^3/d by day 45 under the nitrate loading of 4.0 and 9.6 kg-N/m^3/d, respectively. However, an ongoing decline in the TN removal rate from 13.3 to 1.8 kg-N/m^3/d was observed after increasing the nitrate loading to 15.1 kg-N/m^3/d. The phosphate input into the influent gradually increased from 0.3±0.1 to 4.2±0.1 mg/L, in line with the rise in nitrate loading to fulfill cell synthesis demands (Kong et al., 2016; Qu et al., 2022). Under moderate pH conditions, significant phosphate removal was achieved, following a consistent trend with nitrogen removal. For instance, the average total phosphorus (TP) removal of 1.5±0.4 mg/L was achieved at a TN removal rate of 3.9±0.3 kg-N/m^3/d. This removal increased to 2.2±0.9 mg/L with a higher TN removal rate of 9.5±0.5 kg-N/m^3/d and decreased to 0.6±0.3 mg/L when the TN removal rate dropped to 5.7±3.3 kg-N/m^3/d.

The results demonstrated prominent efficiency in removing both nitrogen and phosphate. At an influent nitrate concentration of 202.8±6.0 mg-N/L and an EBCT of 40 min, the maximum nitrogen removal rate reached 10.3 kg N/m^3/d. This value surpasses the robust performance of S^0PBs (0.08–1.47 kg-N/m^3/d) by 7.0–129 times (Di Capua et al., 2015; Zhang et al., 2022b). And that of S^0FBs (0.9–3.4 kg-N/m^3/d) by 3.0–11.4 times, as indicated in earlier research (Kim et al., 2004a), highlighting the suitability of using S^0FBs for treating nitrate-rich wastewater. A higher TN removal rate was observed when the nitrate loading was raised to 15.1±0.8 kg-N/m^3/d, however, the S^0FB exhibited unstable performance. The probable cause of this instability was attributed to the significant accumulation of nitrite, reaching levels as high as to 219.9 mg-N/L, which can be highly toxic to the denitrifying microorganisms. Meanwhile, the maximum phosphate removal rate reached 0.13 kg-PO_4^{3-}/m^3/d, exceeding that of S^0PBs (0.002–0.005 kg-PO_4^{3-}/m^3/d) by 26–65 times. However, a comparison with S^0FBs was not possible due to insufficiently reported data.

3.5 Microbial community analysis

The structures of the microbial community in the sulfur-attaching biofilm were investigated before start-up (SU) and during the stable operation period (SO), as illustrated in Fig. 5. The two groups exhibited significant differences in the relative abundances of Proteobacteria, Acidobacteriota, Bacteroidota, Choroflexi, Planctomycetota and Campilobacterota at the phylum level. Proteobacteria, Bacteroidota, and Choroflexi were the dominant phyla, representing 40.8%, 15.6%, and 2.1% in the SU group and 58.1%, 23.0%, and 13.3% in the SO group, respectively. Notably, a significant increase to 38.4% in Acidobacteriota was observed in the SU group. As previously reported, the majority of sulfur-oxidizing bacteria belong to the Proteobacteria phylum (Shao et al., 2010). Additionally, Bacteroidota, Chloroflexi, and Planctomycetota contain a substantial population of denitrifying microorganisms (Fernandez et al., 2009; Musat et al., 2010; Zhang et al., 2017).

At the genus level (Fig. 5B), the predominant genera in the SU group were *Acinetobacter*, *unclassified_f_Enterobacteriaceae*, *Pseudomonas*, and *Desulfocapsa*, constituting 29.8%, 20.8%, 12.6%, and 5.9% of the relative abundance, respectively. *Acinetobacter* exhibits a pH tolerance range of 3.0–9.0, allowing its growth during the self-acidification period. Furthermore, acidophilic bacteria like *Pseudomonas*, discovered in the 20th century, have been identified as sulfur-oxidizing bacteria (Zhang et al., 2020). *Desulfocapsa* was observed to facilitate the coupling of elemental sulfur and thiosulfate disproportionation (Finster et al., 1998), illustrating the presence of the SDP process during the start-up period. The dominant genus in the SO group were *Thiobacillus*, *Arenimonas*, and *unclassified_f_Commonadaceae,* presenting high relative abundances of 12.3%, 18.3%, and 17.1%, respectively. *Thiobacillus* is particularly abundant in the S^0AD process, utilizing various reduced sulfur species (e.g., S^0, S^{2-}, $S_2O_3^{2-}$) as electron donors while consuming inorganic carbon sources (e.g., HCO_3^-, CO_2) to facilitate nitrate reduction to N_2 (Alvarez et al., 2007; B et al., 2021; Xu et al., 2021). *Arenimonas* has been verified for its effective nitrate removal in the S^0AD process (Fang et al., 2022), with its relative abundance showing a positive correlation with the TN removal rate (Zhang et al., 2023). Moreover, *Arenimonas* has been reported to be closely related to the anammox process by achieving an effective short-cut denitrification process (Huang et al., 2021; Zhang et al., 2022a). Therefore, the high relative abundance of *Arenimonas* is proposed to be a reason for serious nitrite accumulation during the last period in this study. Compared to the previously observed microbial community in S^0PBs (Sun et al., 2023a; Wang et al., 2022), *Arenimonas* was significantly enriched, which might indicate its significant role in achieving high-rate nitrate removal. Although *Commonadaceae* was not identified at the genus level, this family is commonly observed with a high relative abundance in the S^0AD process, playing a crucial role in denitrification processes (Zhang & Lv, 2021). *Norank_f_A4b* and *PHOS-HE36* were enriched to 3.1% and 3.8% in the SO group, respectively, and have been identified in numerous denitrification systems that actively engage in the sulfur cycle (Shi et al., 2021). *Flavobacterium*, *Thremomonas,* and *Truepera* were detected in the S^0FBs, contributing to denitrification (Yin et al., 2019; Zhang et al., 2021b), with *Thremomonas* even operating under aerobic conditions (Xing et al., 2018; Xlab et al.).

To date, 36 culturable microbial species, such as *Desulfobulbus*, *Desulfocapsa*, *Desulfomonile*, etc., have been identified as capable of conducting the sulfur disproportionation process (Finster et al., 1998; Jackson et al., 2000). Despite the significant contribution of S^0DP to self-acidification and sulfate production, the S^0DP bacteria, identified according to reported species, were not enriched in the SO group of this study. Similar results were also obtained in the previous study that those known S^0DP bacteria were not enriched even in obligative S^0DP bioreactors (Sun et al., 2023b). Therefore, it is reasonable to deduce that certain S^0AD and S^0OX bacteria

might possess the capability to perform S^0DP by altering their metabolic pathways from sulfur oxidation to sulfur disproportionation. However, the functional genes associated with the S^0DP pathways have not yet been identified, which poses challenges in further exploring the underlying mechanism.

4. Conclusions

Self-acidification was observed during the restart of S^0FB, primarily resulting from the dominant sulfur disproportionation process, leading to an excessively low pH that hindered the efficiency of sulfur autotrophic denitrification. Ensuring sufficient alkalinity in both the influent and S^0FB bulk could prevent self-acidification, thereby achieving an effective S^0FB start-up. The S^0FB can achieve nitrogen and phosphate removal capacities one order of magnitude higher than those reported for S^0PB. This study offers a solution for controlling self-acidification during S^0FB start-up and emphasizes the significant potential of utilizing the S^0FB in nitrate-rich wastewater treatment.

E-supplementary data for this work can be found in e-version of this paper online.

Acknowledgments

This study was supported by the National Natural Science Foundation of China (No. 51908540), Open Project of State Key Laboratory of Urban Water Resources and Environment (No. 2021TS14 and QA202324), Shenzhen Science and Technology Program (No. KQTD20190929172630447), Project of Eco-Environmental Technology for Carbon Peak and Neutrality (No. RCEESTDZ-2021-24), Open Project of Key Laboratory of Environmental Biotechnology, CAS (No. kf2021008) and Key Research and Development Project of Shandong Province (No. 2020CXGC011202).

Declaration of Interest Statement

As Huu Hao Ngo a [co-]author on this paper, is an executive editor of Bioresource Technology, he was blinded to this paper during review, and the paper was independently handled by Samir Kumar Khanal as an executive editor."

References

1. Alvarez, R.S., Cardoso, R.B., Salazar, M., Field, J., 2007. Chemolithotrophic Denitrification with Elemental Sulfur for Groundwater Treatment. Water Res., 41(6), 1253–1262.

2. Deng, Y.F., Wu, D., Huang, H., Cui, Y.-X., van Loosdrecht, M.C.M. and Chen, G.H., 2021. Exploration and verification of the feasibility of sulfide-driven partial denitrification coupled with anammox for wastewater treatment. Water Res., 191, 116905.

3. Bai, Y., Wang, S., Zhussupbekova, A., Shvets, I.V., Lee, P.H., Zhan, X.M., 2023. High-rate iron sulfide and sulfur-coupled autotrophic denitrification system: Nutrients removal performance and microbial characterization. Water Res., 231, 119619.

4. Capua, F.D., Lakaniemi, A.M., Puhakka, J.A., Lens, P.N.L., Esposito, G., 2017. High-rate thiosulfate-driven denitrification at pH lower than 5 in fluidized-bed reactor. Chem Eng J., 310(1), 282–291.

5. Chen, F., Li, Z., Ye, Y., Lv, M., Liang, B., Yuan, Y., Cheng, H.-Y., Liu, Y., He, Z., Wang, H., Wang, Y., Wang, A., 2022. Coupled sulfur and electrode-driven autotrophic denitrification for significantly enhanced nitrate removal. Water Res., 220, 118675.

6. Di Capua, F., Lakaniemi, A.-M., Puhakka, J.A., Lens, P.N.L., Esposito, G., 2017. High-rate thiosulfate-driven denitrification at pH lower than 5 in fluidized-bed reactor. Chem Eng J., 310, 282–291.

7. Di Capua, F., Papirio, S., Lens, P.N.L., Esposito, G., 2015. Chemolithotrophic denitrification in biofilm reactors. Chem Eng J., 280, 643–657.

8. Di Capua, F., Pirozzi, F., Lens, P.N.L., Esposito, G., 2019. Electron donors for autotrophic denitrification. Chem Eng J., 362, 922–937.

9. Dong, H., Sun, Y.L., Sun, Q., Zhang, X.N., Wang, H.C., Wang, A.J., Cheng, H.Y., 2023. Effect of sulfur particle morphology on the performance of element sulfur-based denitrification packed-bed reactor. Bioresource Technol., 367, 128238.

10. Fang, Y.K., Wang, H.C., Han, J.L., Li, Z.L., Wang, A.J., 2022. Enhanced nitrogen removal of constructed wetlands by coupling with the bioelectrochemical system under low temperature: Performance and mechanism. J Clean Prod., 350, 131365.

11. Fernandez, N., Sierra-Alvarez, R., Amils, R., Field, J.A., Sanz, J.L., 2009. Compared microbiology of granular sludge under autotrophic, mixotrophic and heterotrophic denitrification conditions. Water Sci Technol., 59 (6), 1227–1236.

12. Finster, K., Liesack, W., Thamdrup, B., 1998. Elemental sulfur and thiosulfate disproportionation by Desulfocapsa sulfoexigens sp. nov., a new. Appl Environ Microb., 64 (1), 119–125.

13. Glass, C., Silverstein, J., 1998. Denitrification kinetics of high nitrate concentration water: pH effect on inhibition and nitrite accumulation. Water Res., 32 (3), 831–839.

14. Gong, L., Huo, M., Yang, Q., Li, J., Ma, B., Zhu, R., Wang, S., Peng, Y., 2013. Performance of heterotrophic partial denitrification under feast-famine condition of electron donor: A case study using acetate as external carbon source. Bioresource Technol., 133, 263–269.

15. Hardisty, D.S., Olyphant, G.A., Bell, J.B., Johnson, A.P., Pratt, L.M., 2013. Acidophilic sulfur disproportionation. Geochim Cosmochim Ac., 113, 136–151.

16. Huang, S., Yu, D., Chen, G., Wang, Y., Tang, P., Liu, C., Tian, Y., Zhang, M., 2021. Realization of nitrite accumulation in a sulfide-driven autotrophic denitrification process: Simultaneous nitrate and sulfur removal. Chemosphere, 278, 130413.

17. Jackson, Bradley, E., McInerney, Michael, J., 2000. Thiosulfate disproportionation by Desulfotomaculum thermobenzoicum. Appl Environ Microb., 66 (8), 3650–3653.

18. Karanasios, K.A., Vasiliadou, I.A., Tekerlekopoulou, A.G., Akratos, C.S., Pavlou, S., Vayenas, D.V., 2016. Effect of C/N ratio and support material on heterotrophic denitrification of potable water in bio-filters using sugar as carbon source. Int Biodeter Biodegr., 111, 62–73.

19. Kim, H.R., Lee, I.S., Bae, J.H., 2004a. Performance of a sulphur-utilizing fluidized bed reactor for post-denitrification. Process Biochem., 39 (11), 1591–1597.

20. Kim, S., Jung, H., Kim, K.S., Kim, I.S., 2004b. Treatment of high nitrate-containing wastewaters by sequential heterotrophic and autotrophic denitrification. J Environ Eng., 130 (12), 1475–1480.

21. Kong, Z., Li, L., Feng, C., Dong, S., Chen, N., 2016. Comparative investigation on integrated vertical-flow biofilters applying sulfur-based and pyrite-based autotrophic denitrification for domestic wastewater treatment. Bioresource Technol., 211, 125–135.

22. Liu, L.H., Koenig, A., 2002. Use of limestone for pH control in autotrophic denitrification: batch experiments. J. Process Biochem., 37 (8), 885–893.

23. Lovley, D.R., Phillips, E.J.P., 1994. Novel Processes for Anaerobic Sulfate Production from Elemental Sulfur by Sulfate-Reducing Bacteria. Appl Environ Microb., 60 (7), 2394–2399.

24. Musat, F., Wilkes, H., Behrends, A., Woebken, D., Widdel, F., 2010. Microbial nitrate-dependent cyclohexane degradation coupled with anaerobic ammonium oxidation. ISME J., 4 (10), 1290–1301.

25. Nancharaiah, Y.V., Venugopalan, V.P., 2011. Denitrification of synthetic concentrated nitrate wastes by aerobic granular sludge under anoxic conditions. Chemosphere., 85 (4), 683–688.

26. Oh, S.E., Kim, K.S., Choi, H.C., Cho, J., Kim, I.S., 2000. Kinetics and physiological characteristics of autotrophic dentrification by denitrifying sulfur bacteria. Water Sci Technol., 42 (3–4), 59–68.

27. Ozkaya, B., Kaksonen, A.H., Sahinkaya, E., Puhakka, J.A., 2019. Fluidized bed bioreactor for multiple environmental engineering solutions. Water Res., 150, 452–465.

28. Qu, J., Bi, F., Li, S., Feng, Z., Li, Y., Zhang, G., Wang, L., Wang, Y., Zhang, Y., 2022. Microwave-assisted synthesis of polyethylenimine-grafted nanocellulose with ultra-high adsorption capacity for lead and phosphate scavenging from water. Bioresource Technol., 362, 127819.

29. Ricardo, B., Cardoso, R., Sierra-Alvarez, P., Rowlette, E., Razo, F., 2006. Sulfide oxidation under chemolithoautotrophic denitrifying conditions. Biotechnol Bioeng., 95 (6), 1148–1157.

30. Ricardo, A.R., Carvalho, G., Velizarov, S., Crespo, J.G., Reis, M.A.M., 2012. Kinetics of nitrate and perchlorate removal and biofilm stratification in an ion exchange membrane bioreactor. Water Res., 46 (14), 4556–4568.

31. Shao, M.F., Zhang, T., Fang, H.H.P., 2010. Sulfur-driven autotrophic denitrification: diversity, biochemistry, and engineering applications. Appl Environ Microb., 88 (5), 1027–1042.

32. Shi, C., Xu, Y., Liu, M., Chen, X., Chen, Y., 2021. Enhanced bisphenol S anaerobic degradation using an NZVI–HA-modified anode in bioelectrochemical systems. J Hazard Mater., 403 (23), 124053.

33. Sun, Y.L., Li, Z.R., Zhang, X.N., Dong, H., Qian, Z.M., Yi, S., Zhuang, W.Q., Cheng, H.Y., Wang, A.J., 2023a. Design and operation insights concerning a pilot-scale S0-driven autotrophic denitrification packed-bed process. Chem Eng J., 470, 144396.

34. Sun, Y.L., Zhai, S.Y., Qian, Z.M., Yi, S., Zhuang, W.Q., Cheng, H.Y., Zhang, X.N., Wang, A.J. 2023b. Managing microbial sulfur disproportionation for optimal

sulfur autotrophic denitrification in a pilot-scale elemental sulfur packed-bed bioreactor. Water Res., 243, 120356.

35. Sun, Y., Feng, L., Li, A., Zhang, X., Yang, J., Ma, F., 2017. Ammonium assimilation: An important accessory during aerobic denitrification of Pseudomonas stutzeri T13. Bioresource Technol., 234, 264–272.

36. Wang, H.C., Liu, Y., Yang, Y.M., Fang, Y.K., Luo, S., Cheng, H.Y., Wang, A.J., 2022. Element sulfur-based autotrophic denitrification constructed wetland as an efficient approach for nitrogen removal from low C/N wastewater. Water Res., 226, 119258.

37. Xing, W., Li, J., Li, D., Hu, J., Deng, S., Cui, Y., Yao, H., 2018. Stable-isotope probing reveals activity and function of autotrophic and heterotrophic denitrifiers in nitrate removal from organic-limited wastewater. Environ Sci Technol., 52 (14), 7867–7875.

38. Xlab, C., Cl, A., Xlc, D., Sl, C., Bx, C., 2020. Intensified pharmaceutical and personal care products removal in an electrolysis-integrated tidal flow constructed wetland. Chem Eng J., 394, 124860.

39. Xu, Y., Liu, Y., Zhang, W., Wang, Z., Li, S., 2018. Optimization of C/N and carbon types on the denitrification biofilter for advanced wastewater treatment. Desalin Water Treat., 119, 107–117.

40. Xu, Z., Qiao, W., Song, X., Wang, Y., 2021. Pathways regulating the enhanced nitrogen removal in a pyrite based vertical-flow constructed wetland. Bioresource Technol., 325, 124705.

41. Yin, W., Wang, K., Wu, D., Xu, J., Zhao, C., 2019. Variation in bacterial communities during landfill leachate treatmenby a modified sequencing batch reactor (SBR). Desalin Water Treat., 140, 365–372.

42. Zhang, L., Lv, J., 2021. Land-use change from cropland to plantations affects the abundance of nitrogen cycle-related microorganisms and genes in the Loess Plateau of China. Appl Soil Eco., 161 (12), 103873.

43. Zhang, L., Qiu, Y.Y., Zhou, Y., Chen, G.H., van Loosdrecht, M.C.M., Jiang, F., 2021a. Elemental sulfur as electron donor and/or acceptor: Mechanisms, applications and perspectives for biological water and wastewater treatment. Water Res., 202, 117373.

459 44. Zhang, X., Wei, D., Zhang, H., He, Y., Zhang, S., Dai, J., Wen, X., 2022a.
460 Comprehensive analysis of the impacts of iron-based nanoparticles and ions on
461 Anammox process. Biochem Eng J., 180, 108371.

462 45. Zhang, X., Zhang, H., Chen, Z., Wei, D., Song, Y., Ma, Y., Zhang, H., 2021b.
463 Achieving biogas production and efficient pollutants removal from nitrogenous
464 fertilizer wastewater using combined anaerobic digestion and autotrophic nitrogen
465 removal process. Bioresource Technol., 339, 125659.

466 46. Zhang, X., Zhang, H., Zhang, N., Ma, Y., Liu, N., Han, G., Wang, Q., 2023.
467 Impacts of exogenous quorum sensing signal molecule-acylated homoserine lactones
468 (AHLs) with different addition modes on Anammox process. Bioresource Technol.,
469 371, 128614.

470 47. Zhang, X.N., Zhu, L., Li, Z.R., Sun, Y.L., Qian, Z.M., Li, S.Y., Cheng, H.Y.,
471 Wang, A.J., 2022b. Thiosulfate as external electron donor accelerating denitrification at
472 low temperature condition in S-0-based autotrophic denitrification biofilter. Environ
473 Res., 210, 113009.

474 48. Zhang, Y., Dai, S., Huang, X., Zhao, Y., Zhang, J., 2020. pH-induced changes in
475 fungal abundance and composition affects soil heterotrophic nitrification after 30 days
476 of artificial pH manipulation. Geoderma. 366, 114255.

477 49. Zhang, Z.J., Qu, Y.Y., Li, S.Z., Feng, K., Wang, S., Cai, W.W., Liang, Y.T., Li, H.,
478 Xu, M.Y., Yin, H.Q., Deng, Y., 2017. Soil bacterial quantification approaches coupling
479 with relative abundances reflecting the changes of taxa. Sci Rep. 7 (1), 4837.

480 50. Zou, G., Papirio, S., Lakaniemi, A.M., Ahoranta, S.H., Puhakka, J.A., 2016. High
481 rate autotrophic denitrification in fluidized-bed biofilm reactors. Chem Eng J. 284,
482 1287–1294.

483

Captions

Table 1. Start-up and operation conditions of S^0FB.

Fig.1. Periodic variation of nitrate concentrations (A), nitrite concentration (B), and pH values (C) in S^0FB.

Fig.2. Periodic variation (A) and pathways (B) of alkalinity consumption in S^0FB.

Fig.3. Periodic variation (A) and pathways (B) of sulfate production, as well as the contributions of different pathways to self-acidification (C) in S^0FB.

Fig.4. Periodic variation (A) and average values (B) of TN removal rate, as well as periodic variation (C) and average values (D) of phosphate removal rate in S^0FB.

Fig.5. Relative abundance of the microbial communities before restart-up and during stable operation at the phylum level (A) and genus level (B).

497 **Table 1.**

498 Start-up and operation conditions of S^0FB

Stages	Influent NO_3^-–N (mg/L)	Influent PO_4^{3-}–P (mg/L)	Alkalinity (mg/L as $CaCO_3$)		pH
Start-up	1st round	20.3±1.4	0.08±0.03	Influent	285.8±48.0	8.5±0.2
				S^0FB bulk (initial value)	150	7.0–7.2
	2nd round	46.6±2.2	0.3±0.07	Influent	2044.6±107.4	8.5±0.2
				S^0FB bulk (initial value)	150	7.0–7.2
	3rd round	50.8±3.5	1.0±0.04	Influent	2235.3±106.8	9.2±0.3
				S^0FB bulk (initial value)	150	7.0–7.2
		49.9±1.4		Influent	3303.3±178.4	8.7±0.2
				49.9S^0FB bulk (initial value)	2000	9.2±0.3
Stable operation		105.9±3.9	1.9±0.1	Following round 3		
		202.8±6.0	3.2±0.3			
		314.5±16.1	4.2±0.1			

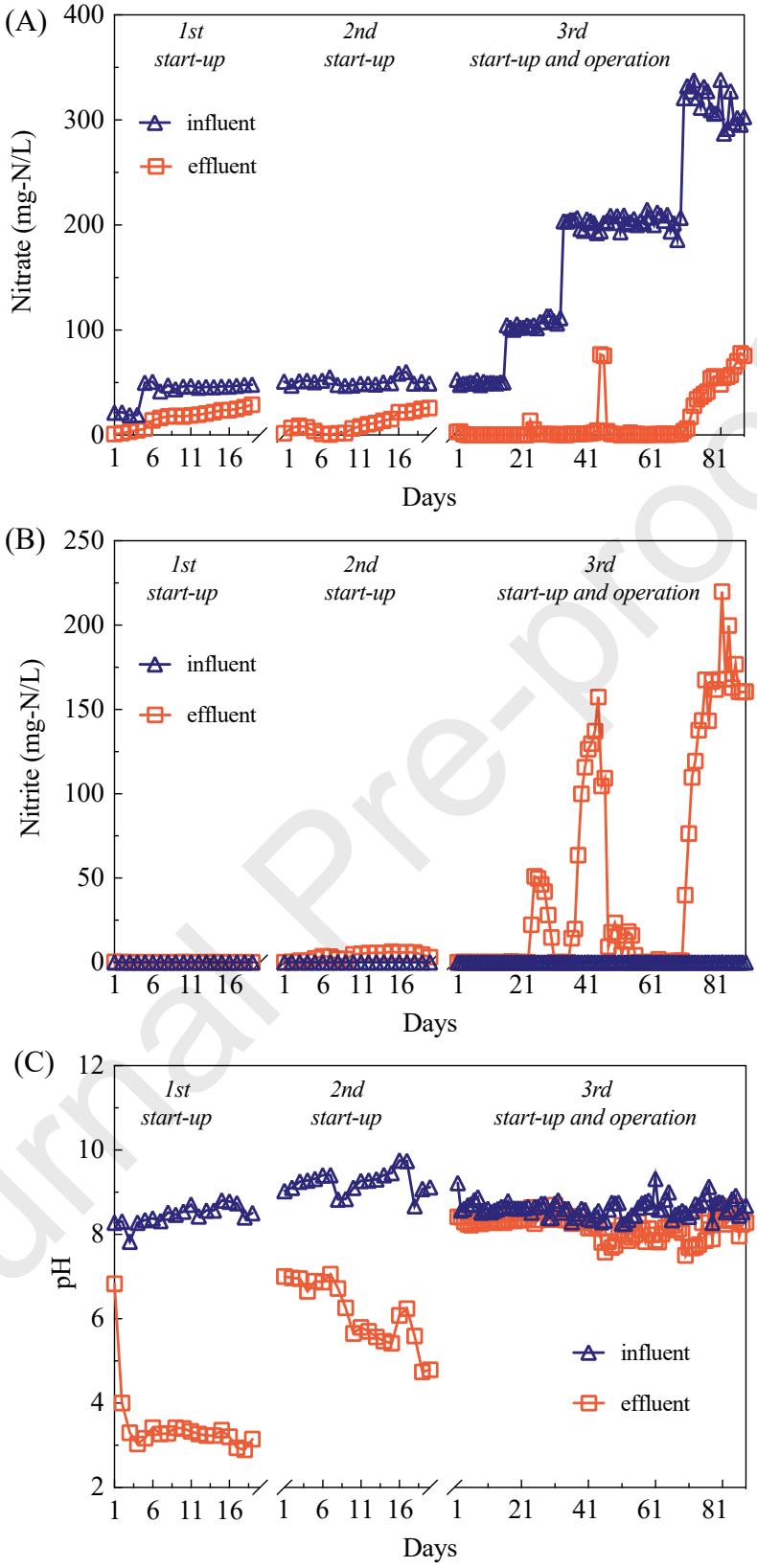

500

501 **Fig.1.** Periodic variation of nitrate concentrations (A), nitrite concentration (B), and
502 pH values (C) in S^0FB.

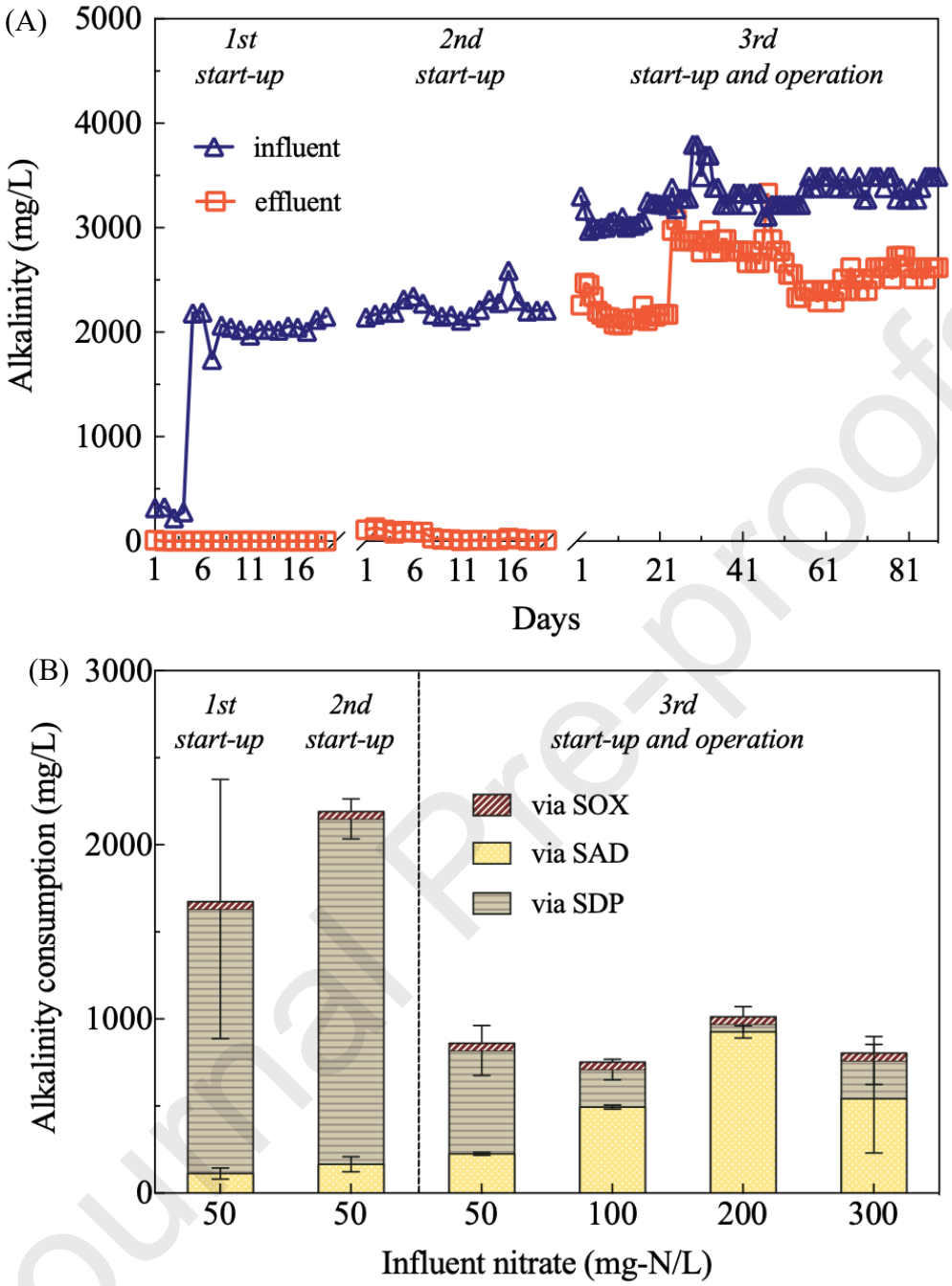

503

504 **Fig.2.** Periodic variation (A) and pathways (B) of alkalinity consumption in S^0FB.

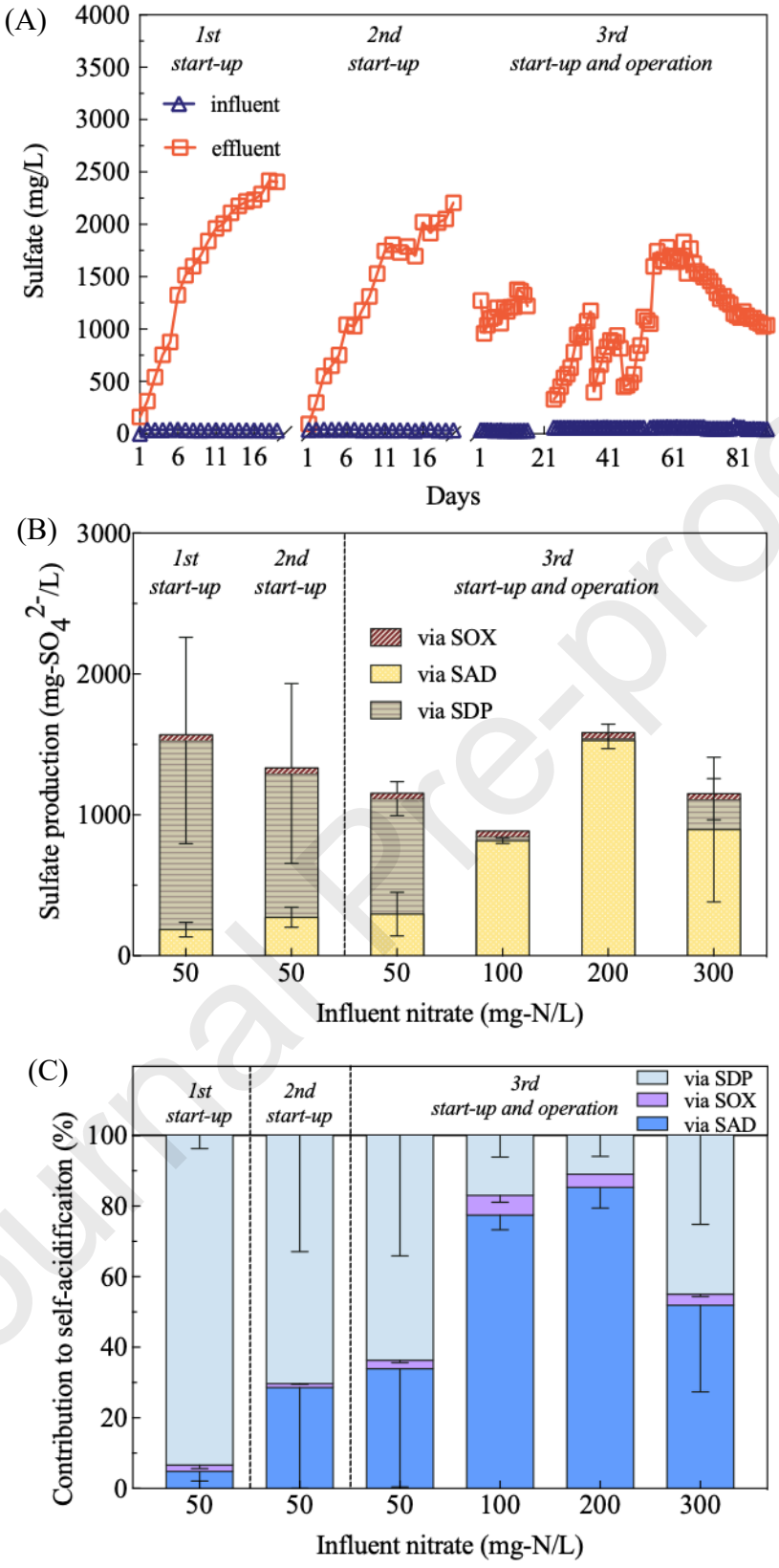

505

506 **Fig.3.** Periodic variation (A) and pathways (B) of sulfate production, as well as the
507 contributions of different pathways to self-acidification (C) in S^0FB.

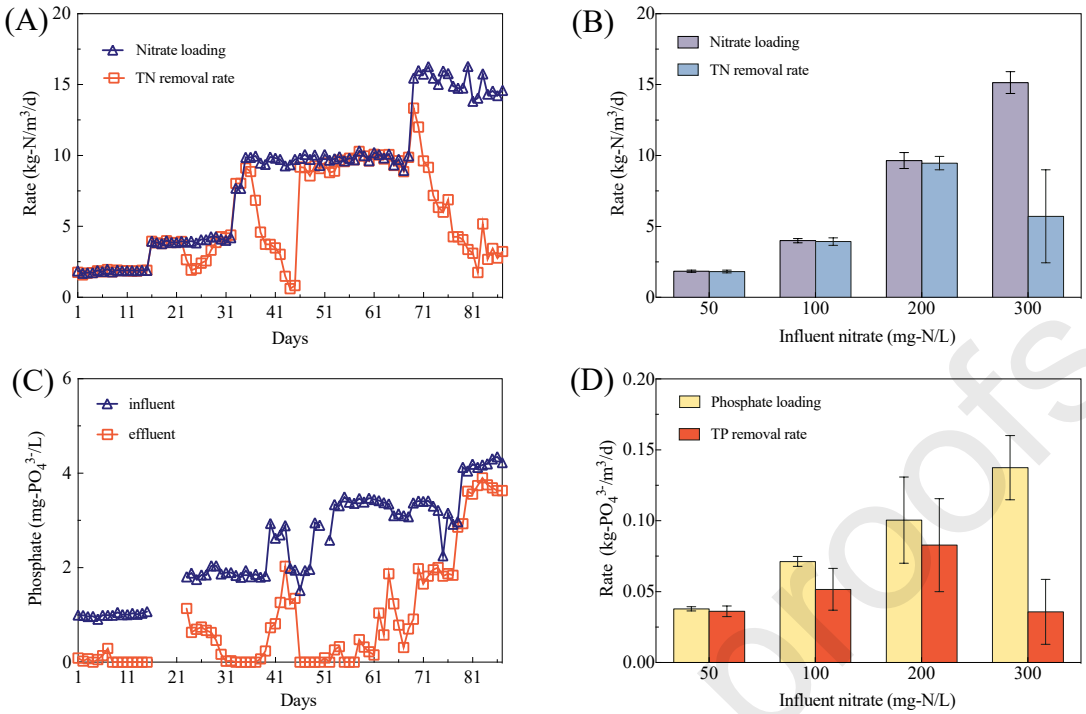

508

509 **Fig.4.** Periodic variation (A) and average values (B) of TN removal rate, as well as
510 periodic variation (C) and average values (D) of TP removal rate in S^0FB.

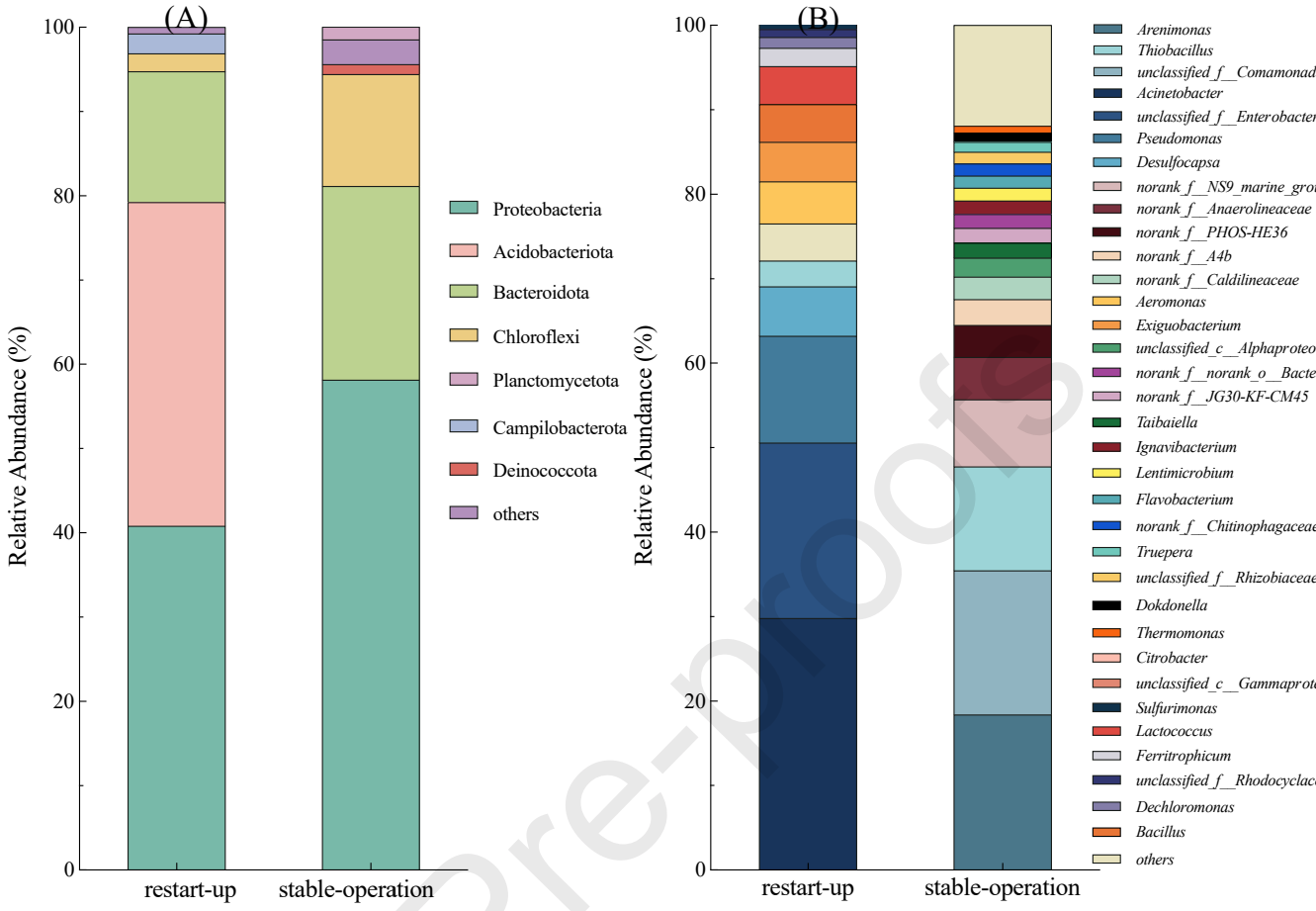

Fig.5. Relative abundance of the microbial communities before restart-up and during stable operation at the phylum level (A) and genus level (B).